DESY 04–083 ISSN 0918–9833

Measurement of the Proton Structure Function F_2 at low Q^2 in QED Compton Scattering at HERA

H1 Collaboration

Abstract

The proton structure function $F_2(x, Q^2)$ is measured in inelastic QED Compton scattering using data collected with the H1 detector at HERA. QED Compton events are used to access the kinematic range of very low virtualities of the exchanged photon, Q^2, down to 0.5 GeV^2, and Bjorken x up to ~0.06, a region which has not been covered previously by inclusive measurements at HERA. The results are in agreement with the measurements from fixed target lepton-nucleon scattering experiments.

Submitted to Physics Letters B

A. Aktas[10], V. Andreev[26], T. Anthonis[4], A. Asmone[33], A. Babaev[25], S. Backovic[37], J. Bähr[37], P. Baranov[26], E. Barrelet[30], W. Bartel[10], S. Baumgartner[38], J. Becker[39], M. Beckingham[21], O. Behnke[13], O. Behrendt[7], A. Belousov[26], Ch. Berger[1], N. Berger[38], T. Berndt[14], J.C. Bizot[28], J. Böhme[10], M.-O. Boenig[7], V. Boudry[29], J. Bracinik[27], V. Brisson[28], H.-B. Bröker[2], D.P. Brown[10], D. Bruncko[16], F.W. Büsser[11], A. Bunyatyan[12,36], G. Buschhorn[27], L. Bystritskaya[25], A.J. Campbell[10], S. Caron[1], F. Cassol-Brunner[22], K. Cerny[32], V. Chekelian[27], C. Collard[4], J.G. Contreras[23], Y.R. Coppens[3], J.A. Coughlan[5], B.E. Cox[21], G. Cozzika[9], J. Cvach[31], J.B. Dainton[18], W.D. Dau[15], K. Daum[35,41], B. Delcourt[28], R. Demirchyan[36], A. De Roeck[10,44], K. Desch[11], E.A. De Wolf[4], C. Diaconu[22], J. Dingfelder[13], V. Dodonov[12], A. Dubak[27], C. Duprel[2], G. Eckerlin[10], V. Efremenko[25], S. Egli[34], R. Eichler[34], F. Eisele[13], M. Ellerbrock[13], E. Elsen[10], M. Erdmann[10,42], W. Erdmann[38], P.J.W. Faulkner[3], L. Favart[4], A. Fedotov[25], R. Felst[10], J. Ferencei[10], M. Fleischer[10], P. Fleischmann[10], Y.H. Fleming[10], G. Flucke[10], G. Flügge[2], A. Fomenko[26], I. Foresti[39], J. Formánek[32], G. Franke[10], G. Frising[1], E. Gabathuler[18], K. Gabathuler[34], E. Garutti[10], J. Garvey[3], J. Gayler[10], R. Gerhards[10,†], C. Gerlich[13], S. Ghazaryan[36], L. Goerlich[6], N. Gogitidze[26], S. Gorbounov[37], C. Grab[38], H. Grässler[2], T. Greenshaw[18], M. Gregori[19], G. Grindhammer[27], C. Gwilliam[21], D. Haidt[10], L. Hajduk[6], J. Haller[13], M. Hansson[20], G. Heinzelmann[11], R.C.W. Henderson[17], H. Henschel[37], O. Henshaw[3], R. Heremans[4], G. Herrera[24], I. Herynek[31], R.-D. Heuer[11], M. Hildebrandt[34], K.H. Hiller[37], P. Höting[2], D. Hoffmann[22], R. Horisberger[34], A. Hovhannisyan[36], M. Ibbotson[21], M. Ismail[21], M. Jacquet[28], L. Janauschek[27], X. Janssen[10], V. Jemanov[11], L. Jönsson[20], D.P. Johnson[4], H. Jung[20,10], D. Kant[19], M. Kapichine[8], M. Karlsson[20], J. Katzy[10], N. Keller[39], J. Kennedy[18], I.R. Kenyon[3], C. Kiesling[27], M. Klein[37], C. Kleinwort[10], T. Klimkovich[10], T. Kluge[1], G. Knies[10], A. Knutsson[20], B. Koblitz[27], V. Korbel[10], P. Kostka[37], R. Koutouev[12], A. Kropivnitskaya[25], J. Kroseberg[39], J. Kückens[10], T. Kuhr[10], M.P.J. Landon[19], W. Lange[37], T. Laštovička[37,32], P. Laycock[18], A. Lebedev[26], B. Leißner[1], R. Lemrani[10], V. Lendermann[14], S. Levonian[10], L. Lindfeld[39], K. Lipka[37], B. List[38], E. Lobodzinska[37,6], N. Loktionova[26], R. Lopez-Fernandez[10], V. Lubimov[25], H. Lueders[11], D. Lüke[7,10], T. Lux[11], L. Lytkin[12], A. Makankine[8], N. Malden[21], E. Malinovski[26], S. Mangano[38], P. Marage[4], J. Marks[13], R. Marshall[21], M. Martisikova[10], H.-U. Martyn[1], S.J. Maxfield[18], D. Meer[38], A. Mehta[18], K. Meier[14], A.B. Meyer[11], H. Meyer[35], J. Meyer[10], S. Michine[26], S. Mikocki[6], I. Milcewicz-Mika[6], D. Milstead[18], A. Mohamed[18], F. Moreau[29], A. Morozov[8], I. Morozov[8], J.V. Morris[5], M.U. Mozer[13], K. Müller[39], P. Murín[16,43], V. Nagovizin[25], B. Naroska[11], J. Naumann[7], Th. Naumann[37], P.R. Newman[3], C. Niebuhr[10], A. Nikiforov[27], D. Nikitin[8], G. Nowak[6], M. Nozicka[32], R. Oganezov[36], B. Olivier[10], J.E. Olsson[10], G.Ossoskov[8], D. Ozerov[25], C. Pascaud[28], G.D. Patel[18], M. Peez[29], E. Perez[9], A. Perieanu[10], A. Petrukhin[25], D. Pitzl[10], R. Plačakytė[27], R. Pöschl[10], B. Portheault[28], B. Povh[12], N. Raicevic[37], Z. Ratiani[10], P. Reimer[31], B. Reisert[27], A. Rimmer[18], C. Risler[27], E. Rizvi[3], P. Robmann[39], B. Roland[4], R. Roosen[4], A. Rostovtsev[25], Z. Rurikova[27], S. Rusakov[26], K. Rybicki[6,†], D.P.C. Sankey[5], E. Sauvan[22], S. Schätzel[13], J. Scheins[10], F.-P. Schilling[10], P. Schleper[10], S. Schmidt[27], S. Schmitt[39], M. Schneider[22], L. Schoeffel[9], A. Schöning[38], V. Schröder[10], H.-C. Schultz-Coulon[14], C. Schwanenberger[10], K. Sedlák[31], F. Sefkow[10], I. Sheviakov[26], L.N. Shtarkov[26], Y. Sirois[29], T. Sloan[17], P. Smirnov[26], Y. Soloviev[26], D. South[10], V. Spaskov[8], A. Specka[29], H. Spitzer[11], R. Stamen[10], B. Stella[33], J. Stiewe[14], I. Strauch[10], U. Straumann[39], V. Tchoulakov[8], G. Thompson[19], P.D. Thompson[3], F. Tomasz[14], D. Traynor[19], P. Truöl[39], G. Tsipolitis[10,40], I. Tsurin[37], J. Turnau[6], E. Tzamariudaki[27], A. Uraev[25], M. Urban[39], A. Usik[26], D. Utkin[25], S. Valkár[32], A. Valkárová[32], C. Vallée[22], P. Van Mechelen[4], N. Van

Remortel[4], A. Vargas Trevino[7], Y. Vazdik[26], C. Veelken[18], A. Vest[1], S. Vinokurova[10], V. Volchinski[36], K. Wacker[7], J. Wagner[10], G. Weber[11], R. Weber[38], D. Wegener[7], C. Werner[13], N. Werner[39], M. Wessels[1], B. Wessling[11], G.-G. Winter[10], Ch. Wissing[7], E.-E. Woehrling[3], R. Wolf[13], E. Wünsch[10], S. Xella[39], W. Yan[10], V. Yeganov[36], J. Žáček[32], J. Zálešák[31], Z. Zhang[28], A. Zhokin[25], H. Zohrabyan[36], and F. Zomer[28]

[1] *I. Physikalisches Institut der RWTH, Aachen, Germany*[a]
[2] *III. Physikalisches Institut der RWTH, Aachen, Germany*[a]
[3] *School of Physics and Astronomy, University of Birmingham, Birmingham, UK*[b]
[4] *Inter-University Institute for High Energies ULB-VUB, Brussels; Universiteit Antwerpen, Antwerpen; Belgium*[c]
[5] *Rutherford Appleton Laboratory, Chilton, Didcot, UK*[b]
[6] *Institute for Nuclear Physics, Cracow, Poland*[d]
[7] *Institut für Physik, Universität Dortmund, Dortmund, Germany*[a]
[8] *Joint Institute for Nuclear Research, Dubna, Russia*
[9] *CEA, DSM/DAPNIA, CE-Saclay, Gif-sur-Yvette, France*
[10] *DESY, Hamburg, Germany*
[11] *Institut für Experimentalphysik, Universität Hamburg, Hamburg, Germany*[a]
[12] *Max-Planck-Institut für Kernphysik, Heidelberg, Germany*
[13] *Physikalisches Institut, Universität Heidelberg, Heidelberg, Germany*[a]
[14] *Kirchhoff-Institut für Physik, Universität Heidelberg, Heidelberg, Germany*[a]
[15] *Institut für experimentelle und Angewandte Physik, Universität Kiel, Kiel, Germany*
[16] *Institute of Experimental Physics, Slovak Academy of Sciences, Košice, Slovak Republic*[e,f]
[17] *Department of Physics, University of Lancaster, Lancaster, UK*[b]
[18] *Department of Physics, University of Liverpool, Liverpool, UK*[b]
[19] *Queen Mary and Westfield College, London, UK*[b]
[20] *Physics Department, University of Lund, Lund, Sweden*[g]
[21] *Physics Department, University of Manchester, Manchester, UK*[b]
[22] *CPPM, CNRS/IN2P3 - Univ Mediterranee, Marseille - France*
[23] *Departamento de Fisica Aplicada, CINVESTAV, Mérida, Yucatán, México*[k]
[24] *Departamento de Fisica, CINVESTAV, México*[k]
[25] *Institute for Theoretical and Experimental Physics, Moscow, Russia*[l]
[26] *Lebedev Physical Institute, Moscow, Russia*[e]
[27] *Max-Planck-Institut für Physik, München, Germany*
[28] *LAL, Université de Paris-Sud, IN2P3-CNRS, Orsay, France*
[29] *LLR, Ecole Polytechnique, IN2P3-CNRS, Palaiseau, France*
[30] *LPNHE, Universités Paris VI and VII, IN2P3-CNRS, Paris, France*
[31] *Institute of Physics, Academy of Sciences of the Czech Republic, Praha, Czech Republic*[e,i]
[32] *Faculty of Mathematics and Physics, Charles University, Praha, Czech Republic*[e,i]
[33] *Dipartimento di Fisica Università di Roma Tre and INFN Roma 3, Roma, Italy*
[34] *Paul Scherrer Institut, Villigen, Switzerland*
[35] *Fachbereich Physik, Bergische Universität Gesamthochschule Wuppertal, Wuppertal, Germany*
[36] *Yerevan Physics Institute, Yerevan, Armenia*
[37] *DESY, Zeuthen, Germany*
[38] *Institut für Teilchenphysik, ETH, Zürich, Switzerland*[j]

[39] Physik-Institut der Universität Zürich, Zürich, Switzerland[j]

[40] Also at Physics Department, National Technical University, Zografou Campus, GR-15773 Athens, Greece
[41] Also at Rechenzentrum, Bergische Universität Gesamthochschule Wuppertal, Germany
[42] Also at Institut für Experimentelle Kernphysik, Universität Karlsruhe, Karlsruhe, Germany
[43] Also at University of P.J. Šafárik, Košice, Slovak Republic
[44] Also at CERN, Geneva, Switzerland
[†] Deceased

[a] Supported by the Bundesministerium für Bildung und Forschung, FRG, under contract numbers 05 H1 1GUA /1, 05 H1 1PAA /1, 05 H1 1PAB /9, 05 H1 1PEA /6, 05 H1 1VHA /7 and 05 H1 1VHB /5
[b] Supported by the UK Particle Physics and Astronomy Research Council, and formerly by the UK Science and Engineering Research Council
[c] Supported by FNRS-FWO-Vlaanderen, IISN-IIKW and IWT and by Interuniversity Attraction Poles Programme, Belgian Science Policy
[d] Partially Supported by the Polish State Committee for Scientific Research, SPUB/DESY/P003/DZ 118/2003/2005
[e] Supported by the Deutsche Forschungsgemeinschaft
[f] Supported by VEGA SR grant no. 2/1169/2001
[g] Supported by the Swedish Natural Science Research Council
[i] Supported by the Ministry of Education of the Czech Republic under the projects INGO-LA116/2000 and LN00A006, by GAUK grant no 173/2000
[j] Supported by the Swiss National Science Foundation
[k] Supported by CONACYT, México, grant 400073-F
[l] Partially Supported by Russian Foundation for Basic Research, grant no. 00-15-96584

1 Introduction

Measurements of deep inelastic lepton-nucleon scattering (DIS) provide information which is crucial to our understanding of proton structure and which has played a decisive role in the development of the theory of strong interactions, Quantum Chromodynamics (QCD). Since the discovery of Bjorken scaling [1] and its violation [2] at fixed target experiments, much progress has been made in extending the kinematic range of measurements in terms of the Bjorken variable x and the modulus of four-momentum transfer squared Q^2. The H1 and ZEUS experiments at the HERA ep collider have shown that the Q^2 evolution of the proton structure function $F_2(x, Q^2)$ is well described by perturbative QCD (pQCD) throughout a wide range in x and Q^2 [3–6]. However, at small Q^2, where the transition takes place into a region in which non-perturbative effects dominate, pQCD is no longer applicable. The data in this region [7,8] are described by phenomenological models such as those derived from the Regge approach.

In order to study this non-perturbative regime, the structure function F_2 has been measured in ep scattering at HERA for very low values of Q^2 using a detector mounted close to the outgoing electron[1] beam direction [8]. The transition region around $Q^2 \sim 1\,\mathrm{GeV}^2$ has been investigated using data taken in dedicated runs with the interaction vertex shifted [7,9]. In this paper a new complementary measurement of F_2 in this kinematic domain is presented, which, following the discussion in [10], utilises ep data with wide angle hard photon radiation, so called QED Compton events.

The data used in this analysis correspond to a luminosity of $9.25\,\mathrm{pb}^{-1}$ and cover the kinematic range of Q^2 between 0.5 and $7\,\mathrm{GeV}^2$. As compared with previous HERA analyses, the range of Bjorken x is significantly extended towards rather large values, between 0.001 and 0.06. This is achieved by introducing a detailed simulation of the hadronic final state at low masses W which includes the resonance region, and through an improved understanding of calorimeter noise.

2 QED Compton Scattering Cross Section

Radiative processes in ep scattering, as depicted in Fig. 1, are of special interest, since the photon emission from the lepton line gives rise to event kinematics which open new ways of investigating proton structure [9–15]. In the present analysis the QED Compton (QEDC) process is considered, which is characterised by low virtuality of the exchanged photon and high virtuality of the exchanged electron. The experimental signature is an approximately back-to-back azimuthal configuration of the outgoing electron and photon. In this configuration it is possible to reconstruct the event kinematics for cases where the exchanged photon virtuality Q^2 is very small.

To describe the process $ep \to e\gamma X$ the standard Lorentz-invariant kinematic variables x and Q^2 have to be defined in a manner which accounts for the additional photon in the final state:

$$Q^2 = -q^2 = -(l - l' - k)^2\,, \qquad x = \frac{Q^2}{2P\cdot(l - l' - k)}\,. \tag{1}$$

[1] The generic name “electron” is used to denote both electrons and positrons.

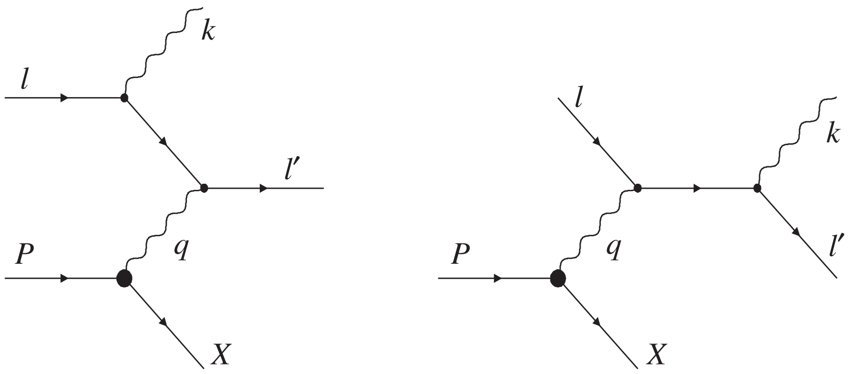

Figure 1: *Lowest order Feynman diagrams for the radiative process $ep \to e\gamma X$ with photon emission from the electron line. Here l and P represent the four-momenta of the incoming electron and the incoming proton, while l', k and X are the four-momenta of the scattered electron, the radiated photon and the hadronic final state, respectively.*

Here l and P are the four-momenta of the incoming electron and the incoming proton, while l' and k represent the four-momenta of the scattered electron and the radiated photon, respectively (Fig. 1). These variables can also be calculated in the usual way using the four-momentum of the hadronic final state. Neglecting the particle masses, the inelasticity y used for the data treatment can be obtained from the relation $Q^2 = xys$, where $s = (l + P)^2$ is the ep centre-of-mass energy squared.

A complete calculation of the QEDC scattering cross section can be found in [16]. Depending on the value of the invariant mass of the hadronic final state, $W = [Q^2(1 - x)/x + m_p^2]^{\frac{1}{2}}$, m_p being the proton mass, three separate contributions to the cross section are considered:

1. **Elastic scattering**, in which the proton stays intact ($W = m_p$). The cross section is calculated from the electric and magnetic form factors of the proton;
2. **Resonance production**, where the total mass of the hadronic final state X lies in the range $m_p < W \lesssim 2\,\text{GeV}$;
3. **Continuum inelastic scattering** at $W \gtrsim 2\,\text{GeV}$. In this region the cross section is defined through the proton structure functions F_2 and F_L.

The dependence on the longitudinal structure function F_L can be neglected in the kinematic range studied in the present analysis, such that the cross section is proportional to F_2. The continuum inelastic QEDC events are thus used to determine the structure function $F_2(x, Q^2)$.

3 Experimental Technique

The analysed events were recorded with the H1 detector [17], which consists of a number of subdetectors designed to perform complementary measurements of particles created in high energy ep collisions. The outgoing electron and photon in QEDC events are selected by requiring two energy depositions (clusters) in the electromagnetic section of the backward[2] lead-fibre calorimeter SpaCal [18]. The SpaCal covers the polar angle range of $153^\circ < \theta < 177^\circ$ and has an electromagnetic energy resolution of $\sigma_E/E = 7\%/\sqrt{E/\mathrm{GeV}} \oplus 1\%$. The final calibration of the electron and photon cluster energies is performed using the double angle reconstruction method [19] with elastic QEDC events [13,20].

The interaction vertex, necessary for polar angle reconstruction, is determined from the intersection of the beam axis with an electron track segment reconstructed in the backward region of the detector. In addition to the electron, the final state photon can also leave a track, if it converts into an electron-positron pair while traversing the tracking chambers. In events in which the electron or the converted photon is scattered into the inner part of the SpaCal, the Backward Silicon Tracker (BST) [21] is used to reconstruct the vertex position. The BST has an angular coverage of $171.5^\circ < \theta < 176.5^\circ$ and a θ resolution of 0.3 mrad. For polar angles $\theta \lesssim 172^\circ$ outside the BST acceptance the Central Inner Proportional Chamber (CIP) [17] is employed in conjunction with the Backward Drift Chamber (BDC) [22] or the SpaCal to determine the vertex coordinates. The BDC is situated in front of the SpaCal and covers a similar angular range. The polar angle resolution for this method of track reconstruction varies between 1.3 and 2 mrad.

For the reconstruction of the kinematic variables Q^2, x and y it is not necessary to distinguish experimentally between the outgoing electron and photon, since the four-momenta of the two particles appear symmetrically in eq. (1). However, at least one of the particles is required to leave a signal in the tracking chambers BST or CIP, in order to determine the interaction vertex coordinates. If both particles produce tracks, the vertex reconstructed with the smaller uncertainty is chosen.

The track reconstruction efficiencies are determined using inclusive DIS data and are found to be 91% on average for the BST and $\gtrsim 99\%$ for the CIP. Due to photon conversions some of the events for which the electron track is not reconstructed remain in the sample. The photon conversion rates amount on average to 21% for the BST and 17% for the CIP acceptance range.

Inelastic QEDC events are distinguished from elastic events by demanding hadronic activity in the detector. The hadronic energy flow is measured in the Liquid Argon Calorimeter (LAr) [17] covering the angular range $4^\circ < \theta < 153^\circ$. Its hadronic energy resolution, as determined in test beam measurements [23], is about $\sigma_E/E = 50\%/\sqrt{E/\mathrm{GeV}} \oplus 2\%$.

The luminosity is measured using low angle bremsstrahlung events by tagging the photon in a photon detector located at $z = -103$ m.

The detector acceptance and background contributions are calculated using Monte Carlo simulations, as described in the following sections. The detector response for events generated by the MC programs is simulated in detail by a program based on GEANT3 [24]. The simulated events are subject to the same reconstruction procedure as the data.

[2]The z axis of the right-handed coordinate system used by H1 is defined by the direction of the incident proton beam with the origin at the nominal ep interaction vertex. Consequently, small scattering angles of the final state electron and photon correspond to large polar angles in the H1 coordinate system.

4 QEDC Event Simulation

QEDC events are simulated by the COMPTON Monte Carlo event generator [16,25], which incorporates a complete calculation of the leading order QEDC cross section. The program also includes higher order corrections for Initial State Radiation in the peaking approximation [26]. For the investigation of inelastic QEDC events an improved version of the COMPTON generator was developed [20] which includes detailed parameterisations for the resonance (Brasse *et al.* [27]) and the continuum (ALLM97 [28]) regions. For the simulation of the hadronic final state the SOPHIA program [29] is used in the range of low Q^2 ($Q^2 < 2\,\mathrm{GeV}^2$) or low masses W ($W < 5\,\mathrm{GeV}$). At higher W and higher Q^2 the Quark Parton Model with subsequent Lund string fragmentation [30] is employed.

The SOPHIA model provides an accurate description of photon-hadron interactions reproducing a large set of available data [29]. The simulation includes the production of the major baryon resonances, direct pion production, multiparticle production based on the Dual Parton Model [31] with subsequent Lund string fragmentation, as well as the diffractive production of the light vector mesons ρ and ω.

5 Background Treatment

A prominent background to inelastic QEDC scattering arises from inclusive DIS events in which one particle from the hadronic final state (typically a π^0) fakes the outgoing photon. At high y, where the hadronic final state lies mostly in the backward region, this process dominates the QEDC signature, hampering a clean QEDC event selection. For this reason the measurement is restricted to relatively low y values (see Sect. 6). Remaining background from inclusive DIS events is modelled using the DJANGO MC generator [32]. This includes LEPTO [33] and ARIADNE [34] for the hard interaction and higher order QCD effects, as well as HERACLES [35] for the calculation of leading order QED radiative corrections. In order to avoid double counting, DJANGO events with hard photons emitted from the lepton line are excluded from the analysis if they fall into the phase space covered by the COMPTON generator.

A priori it cannot be expected that the specific non-perturbative process of isolated (pseudo-) scalar meson production is correctly simulated by an inclusive event generator. Therefore a dedicated study of the DIS background was performed in which the inelastic QEDC selection is extended to events with three electromagnetic SpaCal clusters. One cluster is associated to the scattered electron by matching it to a BST or CIP track segment. Decays of the pseudoscalar mesons π^0 or η into two photons[3] are selected using the invariant mass of the two other clusters. In this study DJANGO is found to provide a reasonable description of events containing π^0 or η mesons. The DIS background is estimated to contribute up to 12% to the total cross section with a systematic uncertainty of 50% of the contribution.

Another source of significant background is Deeply Virtual Compton Scattering (DVCS), in which the final state photon is diffractively produced in the virtual photon proton collision.

[3] The η contribution to the background is small. It is used for this study due to the larger opening angles between the photons in the $\eta \to \gamma\gamma$ decays, compared with the π^0 decays.

DVCS and QEDC are indistinguishable on an event-by-event basis, but differ in the kinematic distributions of the outgoing electron and photon. Both processes can be simulated separately, as the interference between them does not influence the energy and polar angle distributions of the final state particles in the leading twist approximation.

Elastic DVCS events are simulated by the TINTIN generator [36]. The cross section is normalised to the H1 results [37]. The elastic DVCS channel contributes to the measured inelastic QEDC cross section only if noise in the LAr calorimeter is misidentified as hadronic activity. The admixture of such events is negligible.

A sizeable background to the inelastic QEDC cross section arises from proton-dissociative DVCS, which has not yet been measured. In order to estimate the size of this background, it is assumed that the diffractive vertices factorise, such that the ratio of the DVCS cross section with proton dissociation to that with an elastically scattered proton can be modelled using the same ratio for ρ^0 electroproduction [38]. This assumption has been checked in [36]. The inelastic DVCS process is then estimated to contribute 5.5% to the measured cross section and a 100% uncertainty is assigned to the resulting background subtraction.

Further background sources considered are:

- elastic QEDC events, contaminated by electronic noise in the LAr calorimeter. These events contribute $0 - 2\%$ to the measured signal;
- elastic and inelastic dielectron production, modelled using the GRAPE event generator [39]. The contribution varies between 0.5 and 2%;
- inclusive photoproduction, simulated by the PHOJET program [40], which in particular includes the production of the light vector mesons ρ, ω and ϕ. The contribution is $\lesssim 0.5\%$;
- diffractive electroproduction of light vector mesons as well as diffractive J/ψ photo- and electroproduction, all being simulated by the DIFFVM MC generator [41] for both the elastic and the proton-dissociative case. Sizeable backgrounds arise from J/ψ photoproduction ($\lesssim 3\%$) and from ρ electroproduction ($\lesssim 1.5\%$);
- two photon resonance production. The contribution of this process is estimated analytically employing results from [42] and is found to be negligible;
- beam-induced background, estimated using non-colliding particle bunches. This contribution is found to be below 0.5%.

6 Event Selection

The measurement is performed using e^+p data with a centre-of-mass energy of $\sqrt{s} = 301$ GeV. The data were recorded in 1997 and correspond to an integrated luminosity of 9.25 pb^{-1}.

The analysed events were collected by combining two trigger arrangements. The first selects events with two clusters in the electromagnetic part of the SpaCal. This trigger excludes the inner region of the SpaCal, as event rates become large at low scattering angles. The event selection based on this trigger is performed only in a fiducial region in which it is fully efficient. For the present measurement 59% of the events are collected by this trigger.

The remaining events were selected using another trigger arrangement, which selects events with two clusters in the electromagnetic section of the SpaCal with an azimuthal back-to-back topology. Events with significant hadronic activity in the central region of the detector were rejected if more than two tracks were found in the Central Jet Chambers [17]. The usage of this trigger was possible, as in the analysed kinematic domain of low y the final state hadrons are produced mostly at small polar angles.

The trigger efficiencies for both arrangements are determined using independently triggered data. The efficiency of the inelastic event selection by the second trigger is evaluated as a function of the largest polar angle θ_{LAr} of all clusters in the LAr calorimeter which have an energy above 0.5 GeV. It falls from 99% at the minimum θ_{LAr} possible to 79% at $\theta_{\mathrm{LAr}} = 30^\circ$.

For the event selection in the data analysis the following requirements are imposed:

- **Selection criteria for QED Compton events.** The two most energetic clusters in the electromagnetic section of the SpaCal are assumed to be produced by the scattered electron and the radiated photon. The energy of each cluster must exceed 4 GeV, and the sum of both energies must lie between 20 and 30 GeV. The $e\gamma$ acoplanarity defined via $A = |180^\circ - \Delta\phi|$, where $\Delta\phi$ is the azimuthal angle between the electron and photon directions, must be smaller than 45°. Both particles must be found within the acceptance region of either the BST or the CIP. The interaction vertex must be reconstructed, as described in Sect. 3, within 30 cm in z around the nominal interaction point.

- **Additional selection criteria for the inelastic QEDC sample.** At least one particle from the hadronic final state has to be detected with energy above 0.5 GeV in the LAr calorimeter. The energy deposits below 0.5 GeV are classified as noise. The contribution from elastic QEDC events with noise in the LAr calorimeter is further suppressed by requiring that the $e\gamma$ acoplanarity must be larger than 2°. This requirement exploits the fact that the acoplanarity is typically larger for inelastic events than for elastic events due to the different Q^2 dependences of the two processes.

- **Background suppression requirements.** The residual energy in the electromagnetic section of the SpaCal, given by $E_{\mathrm{res}} = E_{\mathrm{tot}} - E_1 - E_2$, where E_{tot} is the total energy and E_1, E_2 are the energies of the QEDC signal clusters, must be below 1 GeV. This cut suppresses DIS, photoproduction, dielectron and vector meson backgrounds. Furthermore, cuts on the shower shape estimators of the two SpaCal clusters are imposed [20] to separate electrons and photons from hadrons. Finally, the phase space is restricted to $y_\Sigma < 0.0062$ (see eq. (2)) to avoid kinematic regions with large contributions from inclusive DIS background.

A brief summary of all selection criteria is given in Table 1. After the selection 1938 events remain in the data sample.

Table 1: *Summary of QEDC selection criteria, as described in the text.*

Purpose	Criterion
Inelastic QEDC signature	$E_1, E_2 > 4\,\text{GeV}$
	$20 < E_1 + E_2 < 30\,\text{GeV}$
	$2^\circ < A < 45^\circ$
	At least one LAr cluster with $E > 0.5\,\text{GeV}$
	$\lvert z_{\text{vtx}}\rvert < 30\,\text{cm}$
Background rejection	$E_{\text{res}} < 1\,\text{GeV}$
	Electromagnetic shower shape requirements
	$y_\Sigma < 0.0062$

7 Event Kinematics and Control Distributions

The redundancy in the measured event properties permits the reconstruction of the variables Q^2, x and y either from the kinematics of the scattered electron and radiated photon or from those of the hadronic final state. Due to the low y values considered in the present analysis, the variables x and y can, however, not be determined solely from the measured electron and photon four-momenta, since their resolution deteriorates as $1/y$. Hence for the kinematic reconstruction the Σ-method [43] is employed, which uses information from the hadronic final state. In addition, this method reduces the influence of higher order radiative effects. With the proton beam energy E_p as well as the sums $\Sigma_h = \sum_i (E - p_z)_i$, where the summation is performed over all hadronic final state objects, and $\Sigma_{e\gamma} = (E - p_z)_e + (E - p_z)_\gamma$, this method yields

$$y_\Sigma = \frac{\Sigma_h}{\Sigma_h + \Sigma_{e\gamma}}\,, \qquad Q^2_\Sigma = \frac{(\vec{p}_{t,e} + \vec{p}_{t,\gamma})^2}{1 - y_\Sigma}\,, \qquad x_\Sigma = \frac{Q^2_\Sigma}{2E_p\Sigma_h}\,. \tag{2}$$

Here, the longitudinal (p_z) and transverse ($\vec{p}_t$) momenta of the measured particles are calculated from their energies (E) and angles neglecting particle masses. As low y values correspond to small polar angles of the final state hadrons, one of the main challenges for the analysis is the correct reconstruction of Σ_h in light of the losses beyond the forward acceptance of the detector. This necessitates a good simulation of hadronisation processes at low invariant masses W.

The quality of the description of the hadronic final state, comprising both the generated hadronic distribution and the subsequent simulation of the detector response, is illustrated in Fig. 2a. The figure shows the ratio of the total transverse momentum of measured hadrons, $p_{t,\text{had}}$, to the total transverse momentum of the $e\gamma$ system, $p_{t,e\gamma}$. The simulation provides a very good description of the data, which is also true for each phase space interval used in the F_2 measurement. Due to losses in the very forward region, outside the acceptance of the LAr calorimeter and the cut at 0.5 GeV on the LAr cluster energy, the distribution peaks at values smaller than one. However, for the calculation of the kinematic variables with the Σ-method, the total $E - p_z$ of the hadrons is used, which is much less sensitive to losses in the beam pipe than $p_{t,\text{had}}$.

The control distribution of y_Σ, shown in Fig. 2b, demonstrates the good quality of both the hadronic simulation and the cross section description given by the COMPTON program down to the lowest y values, even beyond the range used for the measurement. In order to compensate the losses of hadronic energy and thus reduce migration effects, a correction is applied to the measured y which was determined from the difference between the reconstructed and the generated y in simulated events. The correction varies between ~20% on average in the lowest y bins and 0 at the highest y values.

The control distributions in Fig. 3 illustrate the good description of the electron-photon final state provided by the simulation. The energies E_1, E_2 and the polar angles θ_1, θ_2 of the electron and the photon are shown (the subscripts 1 and 2 correspond to the particle with higher and lower energy, respectively), as well as the sum of both energies and the $e\gamma$ acoplanarity. A dip in the polar angle distributions at $\sim 172^\circ$ occurs due to fiducial cuts imposed to ensure a precise description of the BST and CIP acceptance.

8 Results of the Measurement

In order to extract the structure function F_2 the data sample is divided into subsamples corresponding to a grid in y and Q^2. The bin sizes are adapted to the resolution in the measured kinematic quantities such that the stability and purity in all bins shown are greater than 30%. Here, the stability (purity) is defined as the ratio of the number of simulated QEDC events originating from and reconstructed in a specific bin to the number of generated (reconstructed) events in the same bin.

The measured value of the structure function at a given point in Q^2 and $x = Q^2/ys$ is obtained from

$$F_2(x, Q^2) = \frac{N_{\rm data} - N_{\rm bg}}{N_{\rm MC}} F_2^{\rm MC}(x, Q^2) \; . \tag{3}$$

Here, $N_{\rm data}$ represents the number of selected events corrected for the trigger efficiency (Sect. 6), $N_{\rm bg}$ is the sum of all background contributions, estimated as described in Sect. 5, $N_{\rm MC}$ is the number of reconstructed events in the COMPTON simulation rescaled to the luminosity of the data, and $F_2^{\rm MC}$ is the structure function value given by the parameterisation used in the COMPTON simulation. This method takes into account bin-to-bin migration effects, as well as bin-centre and higher order radiative corrections.

Systematic uncertainties are determined by studying the stability of the results under variations of the measured energies and angles, selection efficiencies and background normalisations as well as modifications of the theoretical input. The following systematic errors are estimated:

- The uncertainty on the hadron measurement, which takes into account the errors of the hadronic final state simulation, detector acceptance and LAr calorimeter energy scale, is estimated from the comparison between the data and the simulation in the p_t balance between the reconstructed hadron and electron-photon final states. The contribution to the systematic error varies between 1 and 8%;

- A 10% uncertainty on the energy attributed to noise in the LAr calorimeter is estimated by studying the quality of the simulation of the energy depositions rejected by the noise cut. The contribution to the systematic error varies from 1.5% at the highest y values to 12.5% at the lowest y;
- The uncertainty on the SpaCal energy scale, affecting simultaneously the energies of the electron and the photon, amounts to 0.5% at $E > 17\,\mathrm{GeV}$ and increases linearly towards lower energies up to 2.7% at $E = 4\,\mathrm{GeV}$. This source yields a $1 - 2\%$ error on the F_2 measurement;
- The errors on the F_2 measurement due to the uncertainties in the electron and photon polar angle reconstruction ($0.3 - 2.5\,\mathrm{mrad}$) are typically below 1%;
- The efficiency of the vertex reconstruction is studied using inclusive DIS and elastic QEDC events. The corresponding error contribution to the F_2 measurement is estimated to be 2%;
- Amongst the errors from the background estimation, described in Sect. 5, the main contributions arise from inelastic DVCS (5.5%) and inclusive DIS (up to 6%). The errors from other contributions are $\lesssim 1\%$;
- The statistical errors from the signal and background Monte Carlo event samples contribute up to 5.5% uncertainties on the measurement;
- The luminosity measurement contributes a global 1.5% error;
- The uncertainties on the trigger efficiencies are all below 0.5%. In total they contribute $\lesssim 1\%$ error to the measurement;
- The uncertainty due to radiative corrections, as simulated by the COMPTON generator, amounts to 2%.

The statistical errors lie in the range $6 - 10\%$, while the systematic uncertainties are typically $9 - 12\%$, rising to 18% at the lowest y values. The total errors are obtained by adding the statistical and systematic errors in quadrature.

The F_2 values measured in QED Compton scattering, as summarised in Table 2, are shown in Fig. 4 as a function of x at fixed Q^2 and are compared with other HERA [3,7,8] and fixed target [44–46] data. The present analysis extends the kinematic range of HERA measurements at low Q^2 towards higher x values, thus complementing standard inclusive and shifted vertex measurements. The region covered overlaps with the domain of fixed target experiments. The QEDC F_2 data are consistent with their results. The data are also well described by the ALLM97 parameterisation [28].

9 Summary

The first measurement of the proton structure function F_2 using QED Compton scattering at HERA is presented. The available range of phase space extends down to $Q^2 = 0.5\,\mathrm{GeV}^2$, in the transition region from DIS to photoproduction. Due to an improved treatment of the hadronic final state at small masses W, the measurement extends the low Q^2 kinematic domain of HERA up to $x \sim 0.06$, complementing the analyses of standard inclusive DIS data and data taken with the interaction vertex shifted. The results are in good agreement with data from fixed target lepton-nucleon scattering experiments.

Acknowledgements

We are grateful to the HERA machine group whose outstanding efforts have made this experiment possible. We thank the engineers and technicians for their work in constructing and maintaining the H1 detector, our funding agencies for financial support, the DESY technical staff for continual assistance and the DESY directorate for support and for the hospitality which they extend to the non DESY members of the collaboration.

References

[1] E. D. Bloom *et al.* [SLAC–MIT collaboration], Phys. Rev. Lett. **23** (1969) 930.

[2] D. J. Fox *et al.*, Phys. Rev. Lett. **33** (1974) 1504;
Y. Watanabe *et al.*, Phys. Rev. Lett. **35** (1975) 898.

[3] C. Adloff *et al.* [H1 Collaboration], Eur. Phys. J. C **21** (2001) 33 [hep–ex/0012053].

[4] C. Adloff *et al.* [H1 Collaboration], Eur. Phys. J. C **30** (2003) 1 [hep–ex/0304003].

[5] S. Chekanov *et al.* [ZEUS Collaboration], Eur. Phys. J. C **21** (2001) 443 [hep–ex/0105090].

[6] S. Chekanov *et al.*, [ZEUS Collaboration], DESY–03–214 [hep–ex/0401003].

[7] C. Adloff *et al.* [H1 Collaboration], Nucl. Phys. B **497** (1997) 3 [hep–ex/9703012].

[8] J. Breitweg *et al.* [ZEUS Collaboration], Phys. Lett. B **487** (2000) 53 [hep–ex/0005018].

[9] M. Derrick *et al.* [ZEUS Collaboration], Z. Phys. C **69** (1996) 607 [hep–ex/9510009].

[10] V. Lendermann, H.-C. Schultz-Coulon and D. Wegener, Eur. Phys. J. C **31** (2003) 343 [hep–ph/0307116].

[11] M. W. Krasny, W. Placzek and H. Spiesberger, Z. Phys. C **53** (1992) 687.

[12] J. Blümlein, G. Levman and H. Spiesberger, J. Phys. G **19** (1993) 1695.

[13] T. Ahmed *et al.* [H1 Collaboration], Z. Phys. C **66** (1995) 529.

[14] S. Aid *et al.* [H1 Collaboration], Nucl. Phys. B **470** (1996) 3 [hep–ex/9603004].

[15] A. De Rújula and W. Vogelsang, Phys. Lett. B **451** (1999) 437 [hep–ph/9812231].

[16] A. Courau and P. Kessler, Phys. Rev. D **46** (1992) 117.

[17] I. Abt *et al.* [H1 Collaboration], Nucl. Instrum. Meth. A **386** (1997) 310 and 348.

[18] R. D. Appuhn *et al.* [H1 SpaCal Group], Nucl. Instrum. Meth. A **374** (1996) 149, A **382** (1996) 395 and A **386** (1997) 397.

[19] S. Bentvelsen, J. Engelen and P. Kooijman, in *Proceedings of the Workshop "Physics at HERA", Hamburg, 1991*, DESY (1992) Vol. 1, p. 25;
K. C. Höger, ibid, p. 43.

[20] V. Lendermann, Doctoral Thesis, University of Dortmund, 2002 [DESY–THESIS–02–004].
The COMPTON program can be obtained from:
`http://www.physik.uni-dortmund.de/e5/h1/projekte/compton/` .

[21] W. Eick *et al.*, Nucl. Instrum. Meth. A **386** (1997) 81.

[22] B. Schwab, Doctoral Thesis, Ruprecht Karl University of Heidelberg, 1996.

[23] B. Andrieu *et al.* [H1 Calorimeter Group], Nucl. Instrum. Meth. A **336** (1993) 499.

[24] R. Brun *et al.* [GEANT Team], CERN Program Library Long Writeup W5013.

[25] T. Carli, A. Courau, S. Kermiche and P. Kessler, in *Proceedings of the Workshop "Physics at HERA", Hamburg, 1991*, DESY (1992) Vol. 2, p. 902 and Vol. 3, p. 1468.

[26] E. Etim, G. Pancheri and B. Touschek, Nuovo Cim. B **51S10** (1967) 276;
G. Pancheri, Nuovo Cim. B **60S10** (1969) 321.

[27] F. W. Brasse *et al.*, Nucl. Phys. B **110** (1976) 413.

[28] H. Abramowicz and A. Levy, DESY–97–251 [hep–ph/9712415].

[29] A. Mücke *et al.*, Comput. Phys. Commun. **124** (2000) 290 [astro–ph/9903478].

[30] T. Sjöstrand *et al.*, Comput. Phys. Commun. **135** (2001) 238 [hep–ph/0010017].

[31] A. Capella, U. Sukhatme, C. Tan and J. Tran Thanh Van, Phys. Rept. **236** (1994) 225.

[32] G. A. Schuler and H. Spiesberger, in *Proceedings of the Workshop "Physics at HERA", Hamburg, 1991*, DESY (1992) Vol. 3, p. 1419.

[33] G. Ingelman, in *Proceedings of the Workshop "Physics at HERA", Hamburg, 1991*, DESY (1992) Vol. 3, p. 1366.

[34] L. Lönnblad, Comput. Phys. Commun. **71** (1992) 15.

[35] A. Kwiatkowski, H. Spiesberger and H. J. Möhring, Comput. Phys. Commun. **69** (1992) 155. Also in *Proceedings of the Workshop "Physics at HERA", Hamburg, 1991*, DESY (1992) Vol. 3, p. 1294.

[36] R. Stamen, Doctoral Thesis, University of Dortmund and Free University of Brussels (ULB), 2001 [DESY–THESIS–2001–057].

[37] C. Adloff *et al.* [H1 Collaboration], Phys. Lett. B **517** (2001) 47 [hep–ex/0107005].

[38] C. Adloff *et al.* [H1 Collaboration], Z. Phys. C **75** (1997) 607 [hep–ex/9705014].

[39] T. Abe *et al.*, in *Proceedings of the Workshop "Monte Carlo Generators for HERA Physics", Hamburg, 1998–1999*, p. 566.

[40] R. Engel and J. Ranft, Phys. Rev. D **54** (1996) 4244, [hep–ph/9509373].

[41] B. List and A. Mastroberardino, in *Proceedings of the Workshop "Monte Carlo Generators for HERA Physics", Hamburg, 1998–1999*, p. 396.

[42] W. Kilian and O. Nachtmann, Eur. Phys. J. C **5** (1998) 317 [hep–ph/9712371];
E. R. Berger *et al.*, Eur. Phys. J. C **9** (1999) 491 [hep–ph/9901376].

[43] U. Bassler and G. Bernardi, Nucl. Instrum. Meth. A **361** (1995) 197 [hep–ex/9412004].

[44] L. W. Whitlow *et al.*, Phys. Lett. B **282** (1992) 475 [SLAC–PUB–5442].

[45] M. Arneodo *et al.* [New Muon Collaboration], Nucl. Phys. B **483** (1997) 3 [hep–ph/9610231].

[46] M. R. Adams *et al.* [E665 Collaboration], Phys. Rev. D **54** (1996) 3006.

Table 2: *Measurements of the proton structure function $F_2(x, Q^2)$ in QED Compton scattering, together with fractional statistical ($\delta_{\rm stat}$), systematic ($\delta_{\rm syst}$) and total errors ($\delta_{\rm tot}$). The F_2 values at the points of Q^2, x, y are extracted from the event rates measured in the kinematic bins ΔQ^2, Δy.*

Q^2, GeV^2	x	y	ΔQ^2, GeV^2	Δy	F_2	$\delta_{\rm stat}$,%	$\delta_{\rm syst}$,%	$\delta_{\rm tot}$,%
0.5	0.01578	0.00035	0.1 – 1.0	0.00020 – 0.00062	0.217	8.8	17.9	19.9
0.5	0.00460	0.00120	0.1 – 1.0	0.00062 – 0.00200	0.243	6.3	9.0	11.0
0.5	0.00158	0.00350	0.1 – 1.0	0.00200 – 0.00620	0.236	6.7	11.4	13.2
2.0	0.01841	0.00120	1.0 – 3.0	0.00062 – 0.00200	0.331	7.7	10.0	12.6
2.0	0.00631	0.00350	1.0 – 3.0	0.00200 – 0.00620	0.356	6.3	9.3	11.2
7.0	0.06444	0.00120	3.0 – 20.0	0.00062 – 0.00200	0.418	9.9	14.5	17.6
7.0	0.02209	0.00350	3.0 – 20.0	0.00200 – 0.00620	0.418	7.5	8.9	11.7

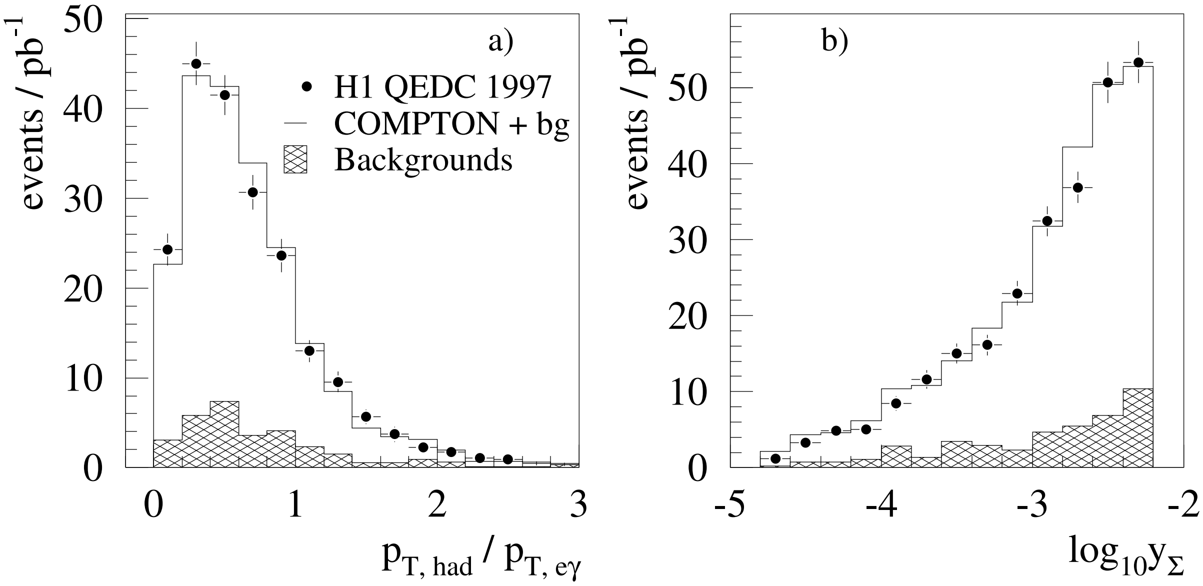

Figure 2: *a) ratio of the total measured transverse momentum of hadrons to the total transverse momentum of the $e\gamma$ system; b) uncorrected y_Σ distribution after applying all selection cuts. The data are depicted by the closed circles. The solid histogram represents the sum of COMPTON MC events and all background contributions. The hatched histogram denotes the sum of all background processes.*

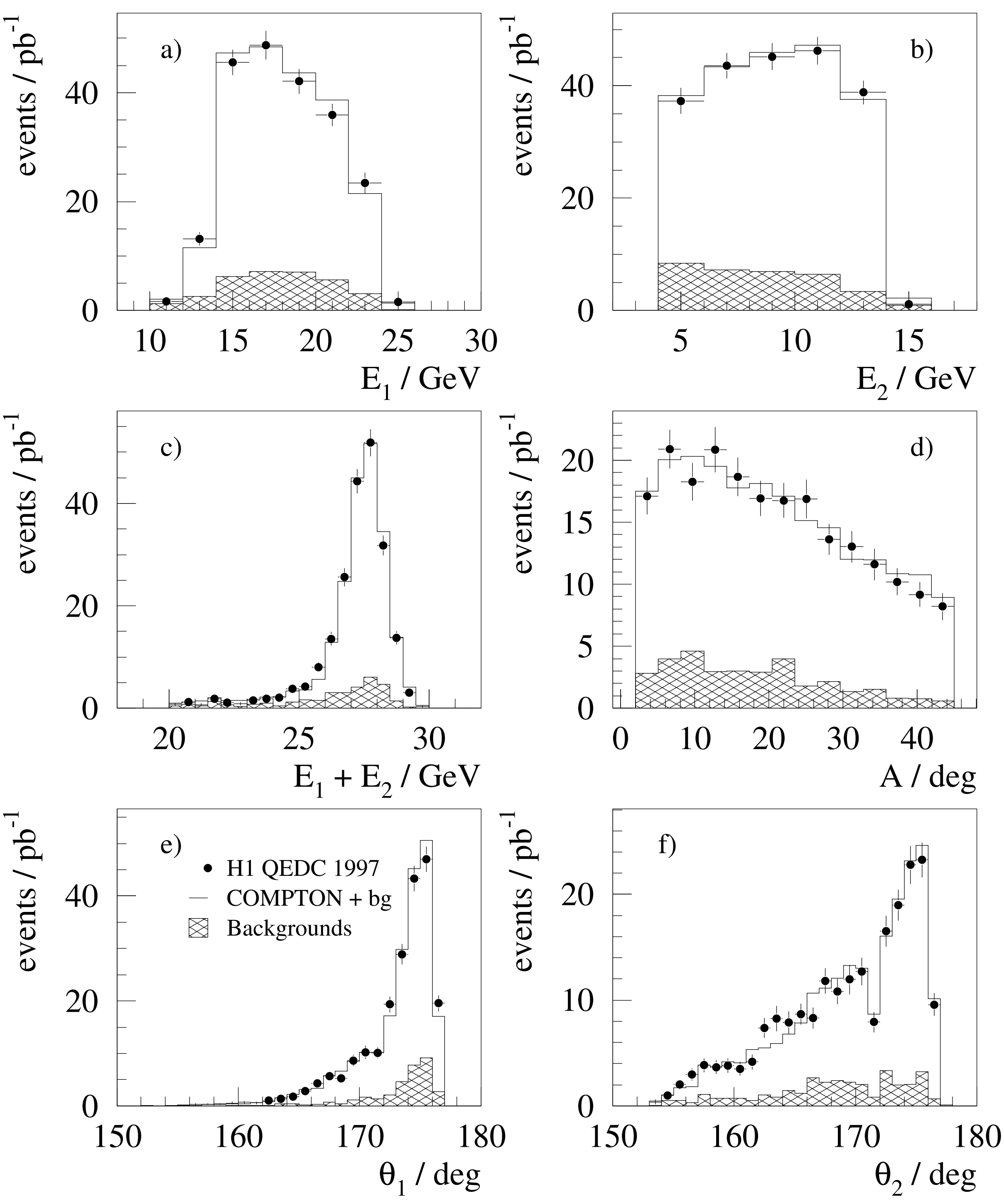

Figure 3: *Control distributions for the measured electron and photon in events used for the measurement: a) energy of the particle with the higher energy; b) energy of the particle with the lower energy; c) sum of both energies; d) $e\gamma$ acoplanarity; e) polar angle of the particle with the higher energy and f) polar angle of the particle with the lower energy. The data are depicted by the closed circles. The solid histogram represents the sum of COMPTON MC events and all background contributions. The hatched histogram denotes the sum of all background processes.*

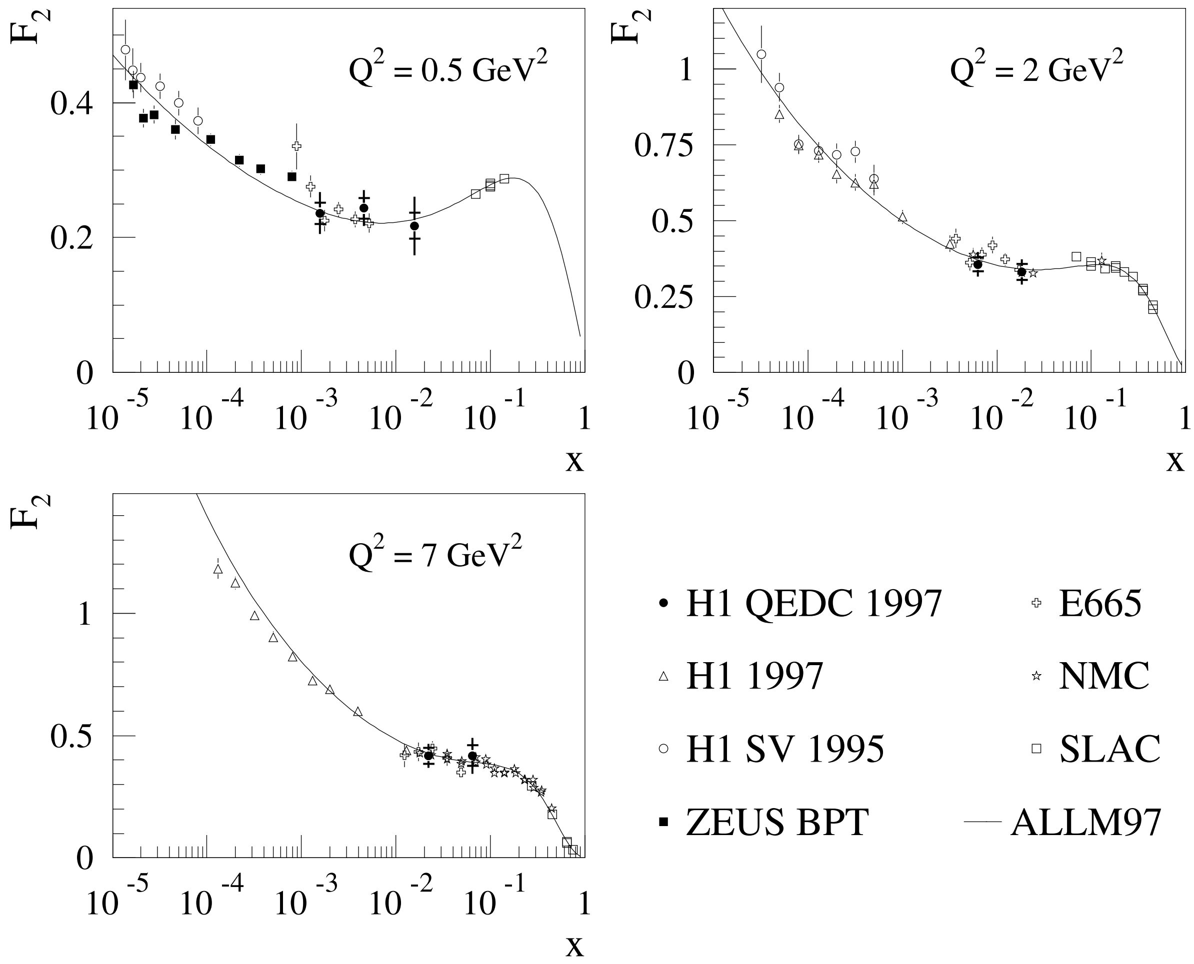

Figure 4: *F_2 measurements from QED Compton scattering by H1 (closed circles), compared with other measurements at HERA (closed squares [8], open triangles [3] and open circles [7]) and fixed target experiments (open squares [44], open stars [45] and open crosses [46]). The inner error bars for the QEDC data represent the statistical errors and the total error bars the statistical and systematic errors added in quadrature. The solid line depicts the ALLM97 parameterisation [28]. The data of the other measurements are shifted to the Q^2 values of the present measurement using the ALLM97 parameterisation.*